Direct Observation of Proton-Neutron Short-Range Correlation Dominance in Heavy Nuclei

M. Duer,[1] A. Schmidt,[2] J.R. Pybus,[2] E.P. Segarra,[2] A.W. Denniston,[2] R. Weiss,[3] O. Hen,[2,*] E. Piasetzky,[1] L.B. Weinstein,[4] N. Barnea,[3] I. Korover,[48] E. O. Cohen,[1] H. Hakobyan,[5] S. Adhikari,[17] Giovanni Angelini,[19] M. Battaglieri,[23] A. Beck,[2,†] I. Bedlinskiy,[27] A.S. Biselli,[15,9] S. Boiarinov,[41] W. Brooks,[5] V.D. Burkert,[41] F. Cao,[13] D.S. Carman,[41] A. Celentano,[23] T. Chetry,[34] G. Ciullo,[21,16] L. Clark,[42] P.L. Cole,[30,20,10] M. Contalbrigo,[21] O. Cortes,[19] V. Crede,[18] R. Cruz Torres,[2] A. D'Angelo,[24,37] N. Dashyan,[46] E. De Sanctis,[22] R. De Vita,[23] A. Deur,[41] S. Diehl,[13] C. Djalali,[34,39] R. Dupre,[26] Burcu Duran,[40] H. Egiyan,[41] A. El Alaoui,[5] L. El Fassi,[31] P. Eugenio,[18] A. Filippi,[25] T.A. Forest,[20] G.P. Gilfoyle,[36] K.L. Giovanetti,[28] F.X. Girod,[41] E. Golovatch,[38] R.W. Gothe,[39] K.A. Griffioen,[45] L. Guo,[17,41] K. Hafidi,[6,46] C. Hanretty,[41] N. Harrison,[41] M. Hattawy,[4] F. Hauenstein,[4] T.B. Hayward,[45] D. Heddle,[12,41] K. Hicks,[34] M. Holtrop,[32] Y. Ilieva,[39,19] D.G. Ireland,[42] B.S. Ishkhanov,[38] E.L. Isupov,[38] H.S. Jo,[29] K. Joo,[13] M.L. Kabir,[31] D. Keller,[44] M. Khachatryan,[4] A. Khanal,[17] M. Khandaker,[33,‡] W. Kim,[29] F.J. Klein,[10] V. Kubarovsky,[41,35] S.E. Kuhn,[4] L. Lanza,[24] G. Laskaris,[2] P. Lenisa,[21] K. Livingston,[42] I .J .D. MacGregor,[42] D. Marchand,[26] N. Markov,[13] B. McKinnon,[42] S. Mey-Tal Beck,[2,†] M. Mirazita,[22] V. Mokeev,[41,38] R.A. Montgomery,[42] A Movsisyan,[21] C. Munoz Camacho,[26] B. Mustapha,[6] P. Nadel-Turonski,[41] S. Niccolai,[26] G. Niculescu,[28] M. Osipenko,[23] A.I. Ostrovidov,[18] M. Paolone,[40] R. Paremuzyan,[32] K. Park,[29,§] E. Pasyuk,[41,7] M. Patsyuk,[2] W. Phelps,[19] O. Pogorelko,[27] Y. Prok,[4,44] D. Protopopescu,[42] M. Ripani,[23] A. Rizzo,[24,37] G. Rosner,[42] P. Rossi,[41,22] F. Sabatié,[11] B.A. Schmookler,[2] R.A. Schumacher,[9] Y. Sharabian,[41] Iu. Skorodumina,[39,38] D. Sokhan,[42] N. Sparveris,[40] S. Stepanyan,[41] S. Strauch,[39,19] M. Taiuti,[23,47] J.A. Tan,[29] N. Tyler,[39] M. Ungaro,[41,35] H. Voskanyan,[46] E. Voutier,[26] R. Wang,[26] X. Wei,[41] M.H. Wood,[8,39] N. Zachariou,[43] J. Zhang,[44] Z.W. Zhao,[14] and X. Zheng[44]

(The CLAS Collaboration)

[1] *School of Physics and Astronomy, Tel Aviv University, Tel Aviv 69978, Israel*
[2] *Massachusetts Institute of Technology, Cambridge, Massachusetts 02139, USA*
[3] *The Racah Institute of Physics, The Hebrew University, Jerusalem, Israe*
[4] *Old Dominion University, Norfolk, Virginia 23529*
[5] *Universidad Técnica Federico Santa María, Casilla 110-V Valparaíso, Chile*
[6] *Argonne National Laboratory, Argonne, Illinois 60439*
[7] *Arizona State University, Tempe, Arizona 85287-1504*
[8] *Canisius College, Buffalo, NY*
[9] *Carnegie Mellon University, Pittsburgh, Pennsylvania 15213*
[10] *Catholic University of America, Washington, D.C. 20064*
[11] *IRFU, CEA, Universit'e Paris-Saclay, F-91191 Gif-sur-Yvette, France*
[12] *Christopher Newport University, Newport News, Virginia 23606*
[13] *University of Connecticut, Storrs, Connecticut 06269*
[14] *Duke University, Durham, North Carolina 27708-0305*
[15] *Fairfield University, Fairfield CT 06824*
[16] *Universita' di Ferrara , 44121 Ferrara, Italy*
[17] *Florida International University, Miami, Florida 33199*
[18] *Florida State University, Tallahassee, Florida 32306*
[19] *The George Washington University, Washington, DC 20052*
[20] *Idaho State University, Pocatello, Idaho 83209*
[21] *INFN, Sezione di Ferrara, 44100 Ferrara, Italy*
[22] *INFN, Laboratori Nazionali di Frascati, 00044 Frascati, Italy*
[23] *INFN, Sezione di Genova, 16146 Genova, Italy*
[24] *INFN, Sezione di Roma Tor Vergata, 00133 Rome, Italy*
[25] *INFN, Sezione di Torino, 10125 Torino, Italy*
[26] *Institut de Physique Nucl'eaire, IN2P3-CNRS, Universit'e Paris-Sud, Universit'e Paris-Saclay, F-91406 Orsay, France*
[27] *Institute of Theoretical and Experimental Physics, Moscow, 117259, Russia*
[28] *James Madison University, Harrisonburg, Virginia 22807*
[29] *Kyungpook National University, Daegu 41566, Republic of Korea*
[30] *Lamar University, 4400 MLK Blvd, PO Box 10009, Beaumont, Texas 77710*
[31] *Mississippi State University, Mississippi State, MS 39762-5167*
[32] *University of New Hampshire, Durham, New Hampshire 03824-3568*
[33] *Norfolk State University, Norfolk, Virginia 23504*
[34] *Ohio University, Athens, Ohio 45701*
[35] *Rensselaer Polytechnic Institute, Troy, New York 12180-3590*

[36] University of Richmond, Richmond, Virginia 23173
[37] Universita' di Roma Tor Vergata, 00133 Rome Italy
[38] Skobeltsyn Institute of Nuclear Physics, Lomonosov Moscow State University, 119234 Moscow, Russia
[39] University of South Carolina, Columbia, South Carolina 29208
[40] Temple University, Philadelphia, PA 19122
[41] Thomas Jefferson National Accelerator Facility, Newport News, Virginia 23606
[42] University of Glasgow, Glasgow G12 8QQ, United Kingdom
[43] University of York, York YO10, United Kingdom
[44] University of Virginia, Charlottesville, Virginia 22901
[45] College of William and Mary, Williamsburg, Virginia 23187-8795
[46] Yerevan Physics Institute, 375036 Yerevan, Armenia
[47] Universita di Genova, Dipartimento di Fisica, 16146 Genova, Italy
[48] Nuclear Research Centre Negev, Beer-Sheva, Israel

We measured the triple coincidence $A(e,e'np)$ and $A(e,e'pp)$ reactions on carbon, aluminum, iron, and lead targets at $Q^2 > 1.5$ (GeV/c)^2, $x_B > 1.1$ and missing momentum > 400 MeV/c. This was the first direct measurement of both proton-proton (pp) and neutron-proton (np) short-range correlated (SRC) pair knockout from heavy asymmetric nuclei. For all measured nuclei, the average proton-proton (pp) to neutron-proton (np) reduced cross-section ratio is about 6%, in agreement with previous indirect measurements. Correcting for Single-Charge Exchange effects decreased the SRC pairs ratio to $\sim 3\%$, which is lower than previous results. Comparisons to theoretical Generalized Contact Formalism (GCF) cross-section calculations show good agreement using both phenomenological and chiral nucleon-nucleon potentials, favoring a lower pp to np pair ratio. The ability of the GCF calculation to describe the experimental data using either phenomenological or chiral potentials suggests possible reduction of scale- and scheme-dependence in cross section ratios. Our results also support the high-resolution description of high-momentum states being predominantly due to nucleons in SRC pairs.

Recent high-momentum transfer measurements have shown that nucleons in the nuclear ground state can form temporary pairs with large relative momentum and small center-of-mass (CM) momentum [1, 2]. These pairs are referred to as short range correlated (SRC) pairs. The formation of SRC pairs in heavy, asymmetric nuclei has implications for momentum sharing between protons and neutrons in these nuclei [3–7], our understanding of the properties of very asymmetric cold dense nuclear systems such as neutron stars [8–10], and the relative modification of proton and neutron structure in nuclei (the EMC effect) [1, 11–17].

Properties of SRC pairs are primarily inferred from measurements of exclusive electron- and proton-induced triple-coincidence hard breakup reactions. In these experiments, a nucleon is knocked out of the nucleus via a high-momentum transfer reaction and detected in coincidence with the scattered probe and a recoil nucleon balancing a large missing momentum. Previous measurements of such $A(e,e'pp)$, $A(e,e'pn)$ and $A(p,2pn)$ reactions in light symmetric nuclei (^{4}He and ^{12}C), showed that neutron-proton (np) SRC pairs are nearly 20 times as prevalent as proton-proton (pp) pairs and, by inference, neutron-neutron (nn) pairs [18–21]. This np-pair dominance was explained as being due to the dominance of the tensor part of the nucleon-nucleon force at high relative momenta [22–25]. See recent reviews in [1, 2].

For nuclei heavier than carbon, the predominance of np-SRC pairs was never extracted directly from measurements of the exclusive $A(e,e'pp)$ and $A(e,e'pn)$ reactions. Instead, it was inferred from measurements of the exclusive $A(e,e'pp)$ and semi-inclusive $A(e,e'p)$ reactions, by assuming that all high missing-momentum nucleons knocked out in the $A(e,e'p)$ reaction are part of SRC pairs [3]. Thus, $A(e,e'p)$ events without a correlated recoil proton were attributed to breakup of np-SRC pairs.

Here we report, for the first time, the simultaneous measurement of exclusive triple coincidence $A(e,e'np)$ and $A(e,e'pp)$ reactions on carbon, aluminum, iron, and lead. The new data confirm the previously deduced np-SRC dominance without the assumptions required by previous analyses [3]. We also show that the new data agree with factorized Generalized Contact Formalism (GCF) calculations [26–28] using both phenomenological and Chiral NN interactions. The agreement between this new measurement and both the previous results and the GCF calculations, supports the high-resolution description of high-momentum nucleons in nuclei as predominantly members of SRC pairs.

In the SRC description of high missing momentum nucleon knockout reactions, the nucleus is described as composed of an off-shell SRC pair (either np, nn or pp) with center of mass (total) momentum $\vec{P}_{cm}$ plus an on-shell $A-2$ residual system with momentum $-\vec{P}_{cm}$ (see Fig. 1). The incident high-energy electron scatters from the nucleus by transferring a single virtual photon, carrying momentum $\vec{q}$ and energy ω, to a single off-shell nucleon in the SRC-pair with initial momentum $\vec{p}_i$ and energy E_i, a process we refer to as quasi-elastic (QE) scattering. If that nucleon does not re-scatter as it leaves the

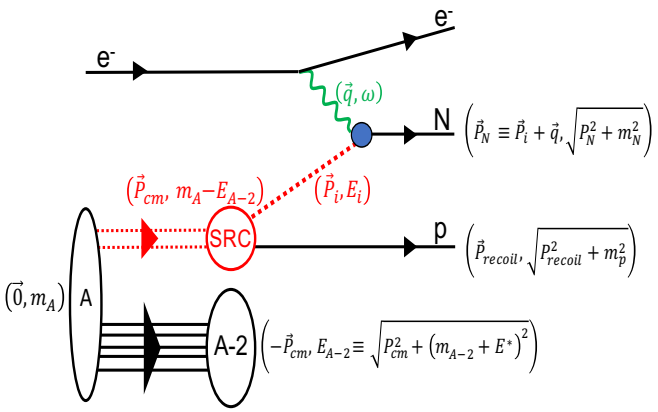

FIG. 1: (color online) Diagrammatic representation and kinematics of the triple-coincidence $A(e,e'Np)$ reaction within the SRC breakup model. Dashed red lines represent off-shell particles. Open ovals represent un-detected systems. Solid black lines represent detected particles. The momentum and energy of the particles is also indicated. See text for details.

nucleus, it will emerge with momentum $\vec{p}_N = \vec{p}_i + \vec{q}$. Thus, we can reconstruct the approximate initial momentum of that nucleon from the measured missing momentum $\vec{p}_i \approx \vec{p}_{miss} = \vec{p}_N - \vec{q}$. The correlated recoil proton is an on-shell spectator that carries momentum $\vec{P}_{recoil} = \vec{P}_{cm} - \vec{P}_{miss}$ and corresponding energy $E_{recoil} = \sqrt{P_{recoil}^2 + m_p^2}$. The undetected residual $A-2$ system has momentum $-\vec{P}_{cm}$ and can have excitation energy E^*.

SRC studies are typically done at $Q^2 = \vec{q}^{\,2} - \omega^2 > 1.5$ (GeV/c)^2, $x_B = Q^2/2m\omega > 1$, (where m is the nucleon mass) anti-parallel kinematics, and missing momentum that exceeds the Fermi momentum, i.e., $|\vec{p}_{miss}| > 300$ MeV/c [3, 6, 21]. According to calculations, non-QE reaction mechanisms (i.e., reactions other than the hard breakup of SRC pairs described above) are suppressed under these conditions [1, 2, 8, 29], and the mechanism of Fig. 1 should be a valid description of the reaction.

Rescattering of the outgoing struck nucleon (final state interactions or FSI) might alter the final state of the reaction. This rescattering includes contributions from nuclear transparency (flux reduction), small angle nucleon rescattering, and single-charge exchange (SCX). However, these effects are significantly reduced in cross-section ratios as compared to absolute cross-sections [1, 30–32]. In addition, at the relevant high-Q^2, the cross-sections approximately factorize and calculations of FSI, including both outgoing-nucleon rescattering and SCX, are done using an Eikonal approximation in a Glauber framework, which was shown to agree well with data (see [2, 29, 31, 33–39] and references therein). These calculations show that small-angle rescattering (i.e., FSI that do not lead to a reduction of flux) is largely confined to within the nucleons of the pair [8, 29, 31, 40]. Such rescattering does not change the isospin structure of SRC pairs, which is the focus of this analysis.

The theoretical description of high-momentum transfer measurements presented above constitutes a valid simple reaction picture that is consistent with both data and various ab-initio calculations [1, 2, 41]. However, it is not the only possible description of such reactions. Utilizing unitary freedom, one can always shift the complexities of explicit two-body correlations from nuclear wave functions to the interaction operators without changing the measured cross-sections (i.e., shifting from a simple one-body operator acting on a complicated ground state with SRC pairs, to a simple ground state with complicated many-body interaction operators). Therefore, there is no unique way to separate the description of the nuclear ground state from that of the reaction mechanism (see, e.g., discussion in Ref. [42] for the deuteron photodisintegration case). For clarity of the discussion, this work focuses on a high-resolution reaction picture, using one-body operators. The results presented here can, however, be used to also constrain theoretical calculations done using the low-resolution many-body operators approach.

The data presented here were collected in 2004 in Hall B of the Thomas Jefferson National Accelerator Facility (Jefferson Lab) in Virginia, USA, and are re-analyzed here as part of the Jefferson Lab data-mining initiative [43]. The experiment used a 5.01 GeV electron beam incident on deuterium, carbon, aluminum, iron, and lead targets [44], and the CEBAF Large Acceptance Spectrometer (CLAS) [45] to detect the scattered electron, the knocked-out proton or neutron, and the recoil proton.

CLAS used a toroidal magnetic field and six independent sets of drift chambers, time-of-flight (TOF) scintillation counters, Cherenkov Counters (CC), and Electromagnetic Calorimeters (EC). Charged particle momenta were inferred from their reconstructed trajectories as they bend due to the influence of the toroidal magnetic field. Electrons were identified by requiring a signal in the CC and a characteristic energy deposition in the EC. Pro-

TABLE I: The $(e,e'Np)$ event selection cuts. Also shown is the sensitivity of the pp/np ratios to variations of the cuts. *Both leading nucleon cuts were varied simultaneously.

Cut	Cut Sensitivity [%] Range	C	Al	Fe	Pb
$x_B > 1.1$	± 0.05	1.5	1.9	1.4	1.7
$0.62 < \lvert\vec{p}_N\rvert/\lvert\vec{q}\rvert < 1.1$	*± 0.1	2.7	2.5	2.3	2.2
$\theta_{Nq} < 25^\circ$	*$\pm 5^\circ$				
$m_{miss} < 1.175$ GeV/c^2	± 0.02 GeV/c^2	2.4	2.3	3.1	2.0
$0.4 < p_{miss} < 1$ GeV/c	± 0.025 GeV/c	2.6	2.8	2.1	2.1
$p_{recoil} > 0.35$ GeV/c	± 0.025 GeV/c	2.4	2.6	2.3	2.7
SC Deposited Energy	cut ON/OFF	0.2	3.2	1.0	2.3
Total		5.3	6.3	5.2	5.4

TABLE II: Measured $[A(e,e'pp)/2\sigma_{ep}]/[A(e,e'np)/\sigma_{en}]$ reduced cross-section ratios in percent units and their uncertainties divided into two recoil proton momentum bins. The first uncertainty is statistical while second is systematical. See text for details.

A	$\lvert P_{recoil}\rvert$ [GeV/c]	
	0.3 - 0.6	0.6 - 1.0
C	5.33 ± 0.65 ± 0.35	7.87 ± 1.68 ± 0.70
Al	5.33 ± 1.09 ± 0.33	8.76 ± 3.63 ± 1.05
Fe	5.88 ± 0.68 ± 0.34	6.53 ± 1.16 ± 0.41
Pb	5.71 ± 1.49 ± 0.39	6.70 ± 1.93 ± 0.40

tons and pions were identified by comparing their measured flight times and momenta. For low-momentum particles ($p < 700$ MeV/c), proton/pion separation was further improved by requiring the protons to deposit more than 15 MeV in the 5-cm thick TOF counters. Neutrons were identified by observing interactions in the forward EC (covering about 8° to 45°) with no associated hit in the corresponding TOF counter and no matching charged-particle track in the drift chambers. The angle- and momentum-dependent neutron detection efficiency and momentum reconstruction resolution were measured using the exclusive $d(e,e'p\pi^+\pi^-)n$ and $d(e,e'p\pi^+\pi^-n)$ reactions. See the on-line supplemental information of Refs. [3, 6] for details of the analysis.

We selected high missing-momentum $(e,e'p)$ and $(e,e'n)$ events (i.e., events with a "leading" proton or neutron) following the procedure of Ref. [6] using the cuts detailed in Table I. We further required the detection of a lower-momentum recoil-proton ($350 \le |\vec{p}_{recoil}| \le 1000$ MeV/c) to obtain $(e,e'pp)$ and $(e,e'np)$ events. Since the recoil protons had relatively low momentum, following [3] we corrected their momenta for energy loss in the target and the CLAS detector.

As CLAS uses an open (e,e') trigger, $A(e,e'pp)$ and $A(e,e'np)$ reactions were measured simultaneously. We matched the $A(e,e'pp)$ and $A(e,e'np)$ acceptances by considering only leading nucleons which were detected in the phase-space region with good acceptance for both protons and neutrons. To extract the $A(e,e'pp)$ / $A(e,e'np)$ cross-section ratio from the measured event yields, we weighted each event by the inverse of the leading-nucleon detection efficiency.

Figure 2 shows the resulting reduced cross-section ratio

$$R = \frac{Y(A(e,e'pp))/2\sigma_{ep}}{Y(A(e,e'np))/\sigma_{en}} \qquad (1)$$

for all measured nuclei (where Y is the efficiency-corrected yield, and σ_{ep} and σ_{en} are the elementary electron-proton and electron-neutron cross sections, respectively [46]), divided into two bins of recoil proton momenta ($350-600$ and $600-1000$ MeV/c). The weighting factors of $1/(2\sigma_{ep})$ and $1/\sigma_{en}$ were applied event-by-event to account for the different elementary electron-nucleon

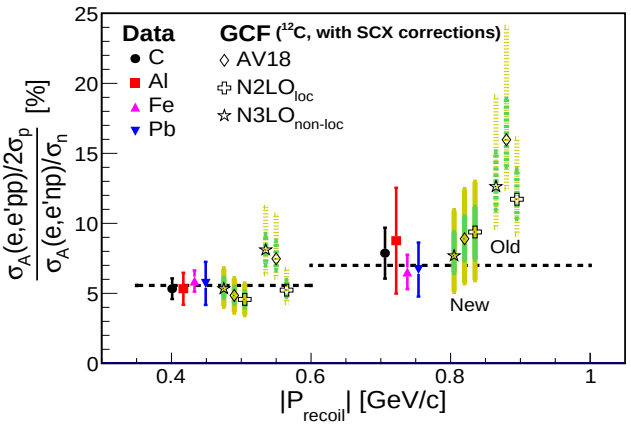

FIG. 2: (color online) Extracted reduced cross-section ratios R for pp to np SRC pair knockout as a function of recoil proton momenta. Different filled symbols mark different nuclei. The black dashed lines show the average cross-section ratio for all four nuclei and their horizontal extents show the width of each recoil proton momenta bin. The open symbols show the results of GCF calculations for ^{12}C using three different NN interactions. The inner (green) and outer (yellow) bands represent the 68% and 95% confidence ranges of the calculation. The points with dashed error bars correspond to GCF calculations using the "old" pp to np contact ratios of Ref. [28] and the points with the solid error bars use "new" contact ratios fit to this data set. See text for details.

cross sections and the different nucleon counting. The error bars show both statistical and systematical uncertainties added in quadrature. The latter include sensitivity of the extracted cross-section ratio to the event selection cuts detailed in Table I, uncertainties in the neutron and proton detection efficiencies, and a small difference for the leading proton and neutron transparencies in iron and lead [31, 47] (see table I in the online supplementary materials). Numerical values for the extracted cross-section ratios are listed in Table II.

The reduced cross-section ratio R in each bin is A-independent, and increases from an average of $5.5\pm0.4\%$ at the lower P_{recoil} bin to $7.0\pm0.9\%$ at the higher bin. Its small value is consistent with np-SRC pairs being $15-20$ times more abundant than pp-SRC pairs. The increase between the two bins is also consistent with the expected increased contribution of pp-SRC pairs at higher relative momenta where the tensor part of the nuclear interaction is less predominant [21].

In order to extract the ratio of np to pp pairs in the nucleus from the reduced cross-section ratio, we need to correct for the attenuation and SCX interactions (e.g., (n,p) and (p,n) reactions) of the nucleons as they exit the nucleus. At the measured outgoing nucleon momenta, the pp and nn elastic scattering cross-sections are similar, so nucleon attenuation largely cancels in the $A(e,e'np)$ / $A(e,e'pp)$ cross-section ratio (see [31] for details). However, SCX can increase the observed re-

duced cross-section ratio. Because there are so many more np- than pp-SRC pairs, np pair knockout, followed by an (n,p) charge-exchange reaction, could comprise a large fraction of the measured $A(e,e'pp)$ events. Correcting for this effect will decrease the extracted ratio of pp- to np-SRC pairs relative to the measured reduced cross-section ratio R. Thus, R is an upper limit on the pp- to np-SRC pairs ratio.

We calculated scattering cross sections for the reaction diagram shown in Fig. 1 using the factorized GCF model [28]. These GCF calculations use SRC-pair relative momentum distributions calculated with a given NN potential (which are the same for all nuclei), the measured P_{cm} distributions [48], and the relative abundances of np, pp, and nn pairs (i.e., the "contacts") in a given nucleus (see online Supplementary Materials for details). The P_{cm} distributions, that describe the influence of the $A-2$ nuclear system on the SRC pairs, can also be obtained from mean-field calculations [36, 49]. These calculated P_{cm} distributions are consistent with the experimentally extracted ones [48]. We therefore do not expect them to have significant scale- and scheme-dependence.

We used Glauber-based calculations to estimate the model- and kinematics-dependent SCX corrections [31]. We applied these corrections in two ways, to correct the GCF cross-section calculations and compare them to the uncorrected data, and also to correct our data in order to directly extract the relative abundance of pp- and np-SRC pairs. As the Glauber calculations describe the influence of the $A-2$ system on the measured reactions, and are based on measured NN scattering cross-sections, we also do not expect them to have significant scale- and scheme-dependence.

Figure 2 shows the measured reduced cross section ratios (without SCX corrections) compared with SCX-corrected GCF cross-section ratio calculations. The GCF calculations are done for ^{12}C, following Ref. [28] using three NN potentials: the phenomenological AV18 [50], a chiral EFT local N2LO(1.0) [51, 52], and a chiral EFT non-local N3LO(600) [53]. The uncertainties in the calculation include contributions from the measured width of the SRC pair cm motion ($\sigma_{cm} = 150 \pm 20$ MeV/c) [48], the residual $A-2$ excitation energy ($E^* = 0$ to 30 MeV), SCX probabilities (see table I in the online supplementary materials), values of the contact terms, and off-shell electron-nucleon cross-section model (σ_{CC1} and σ_{CC2} from Ref. [54], using the form factor parameterization of Ref. [55]).

We calculated the cross section ratios for two different sets of pp (spin-0) to np (spin-1 only) contact ratios. The 'Old' ones used those previously determined in Ref. [28] while the 'New' ones used contacts directly fitted to the new data presented here. See online supplementary materials for details.

The previously determined [28] pp to np contact ratios for the AV18, local N2LO, and non-local N3LO interactions are: $7.1\% \pm 1.5\%$; $5.2\% \pm 1.1\%$; and $4.0\% \pm 0.8\%$ respectively. The contact values fitted to this data are significantly lower: $3.0\% \pm 0.8\%$; $3.6\% \pm 1.0\%$; and $1.9\% \pm 0.5\%$ for the three different potentials. A large part of this reduction (factor of about 1.7) is due to the more complete SCX corrections applied here, as compared to that available ten years ago [56] for the data used in Ref. [28].

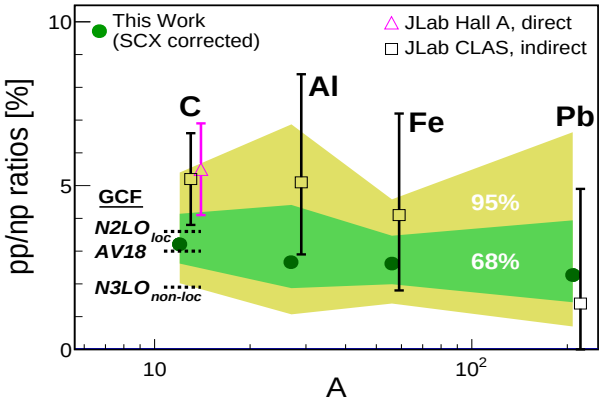

FIG. 3: (color online) Extracted ratios of pp- to np-SRC pairs plotted versus atomic weight A. The filled green circles show the ratios of pp- to np-SRC pairs extracted from $(e,e'pp)$ / $(e,e'pn)$ cross-section ratios corrected for SCX using Eq. 2. The shaded regions mark the 68% and 95% confidence limits on the extraction due to uncertainties in the measured cross-section ratios and SCX correction factors (see online supplementary materials for details). The magenta triangle shows the carbon data of [20], which were also corrected for SCX. The open black squares show the indirect extraction of Ref. [3]. The uncertainties on both previous extractions mark the 68% (i.e. 1σ) confidence limits. The horizontal dashed lines show the ^{12}C GCF-calculated contact ratios for different NN potentials using contact values fitted directly to the measured cross-section ratios. See text for details.

Figure 3 shows the alternative approach where we directly correct the data for SCX effects. This allows determining the pp to np fraction with different and somewhat simplified assumptions than those used by the GCF calculation. For this we consider all recoil proton momenta and express the relative abundance of pp- to np-SRC pairs as (see derivation in the online supplementary materials):

$$\frac{\#pp\text{-}SRC}{\#np\text{-}SRC} = \frac{1}{2}\frac{2RP_A^{np} - P_A^{[n]p} - P_A^{p[n]}/\sigma_{p/n}}{P_A^{pp} - 2\sigma_{p/n}RP_A^{[p]p} - 2R\eta_A P_A^{n[n]}}, \quad (2)$$

where $\eta_A = \frac{\#nn\text{-}SRC}{\#pp\text{-}SRC}$ and R is reduced cross section ratio of Eq. 1. P_A^{NN} is the probability for scattering off an NN pair without subsequent SCX, and $P_A^{[N]N}$ and $P_A^{N[N]}$ are the probabilities for scattering off an NN pair and having either the leading or recoil nucleon undergo SCX, respectively. The values and uncertainties of the parameters used in Eq. 2 are listed in table I of the online supplementary materials.

While the current analysis uses the SCX calculations of Ref. [31] and the formalism detailed in the online supplementary materials, other calculations for these corrections can be applied in the future. See online supplementary materials for detailes on the numerials evaluation of Eq. 2 and its uncertainty.

These SCX-corrected pp/pn ratios agree within uncertainty with the ratios previously extracted from $A(e,e'pp)$ and $A(e,e'p)$ events [3], which assumed that all high-missing momentum nucleons belong to SRC pairs. In addition, the SCX-corrected pp/np ratio is in better agreement with the GCF contacts fitted here but is not inconsistent with those determined in Ref. [28]. This is a significant achievement of the GCF calculations that opens the way for detailed data-theory comparisons. This will be possible using future higher statistics data that will allow finer binning in both recoil and missing momenta.

The pp/np ratios measured directly in this work are somewhat lower than both previous indirect measurements on nuclei from C to Pb[3], and previous direct measurements on C [20]. This is due to the more sophisticated SCX calculations used in this work [31] compared to the previous ones [56]. This is consistent with the lower values of the pp to np contact extracted from GCF calculations fit to this data mentioned above.

To conclude, we report the first measurements of high momentum-transfer hard exclusive np and pp SRC pair knockout reactions off symmetric (^{12}C) and medium and heavy neutron-rich nuclei (^{27}Al, ^{56}Fe, and ^{208}Pb). We find that the reduced cross-section ratio for proton-proton to proton-neutron knockout equals $\sim 6\%$, consistent with previous measurements off symmetric nuclei. Using model-dependent SCX corrections, we also extracted the relative abundance of pp- to pn-SRC pairs in the measured nuclei. As expected, these corrections reduce the pp-to-np ratios to about 3%, so that the measured reduced cross-section ratios are an upper limit on the relative SRC pairs abundance ratios.

The data also shows good agreement with GCF calculations using phenomenological as well as local and non-local chiral NN interactions, allowing for a higher precision determination of nuclear contact ratios and a study of their scale- and scheme-dependence. While the contact-term ratios extracted for phenomenological and local-Chiral interactions are consistent with each other, they are larger than those obtained for the non-local Chiral interaction examined here. Forthcoming data with improved statistics will allow mapping the missing and recoil momentum dependence of the measured ratios. This will facilitate detailed studies of the origin, implications, and significance of such differences.

Previous work [3] measured $A(e,e'p)$ and $A(e,e'pp)$ events and derived the relative probabilities of np and pp pairs assuming that all high-missing momentum $A(e,e'p)$ events were due to scattering from SRC pairs. The agreement between the pp/np ratios directly measured here and those of the previous indirect measurement, as well as with the factorized GCF calculations, strengthens the np-pair dominance theory and also lends credence to the previous assumption that almost all high-initial-momentum protons belong to SRC pairs in nuclei from C to Pb.

We acknowledge the efforts of the staff of the Accelerator and Physics Divisions at Jefferson Lab that made this experiment possible. We are also grateful for many fruitful discussions with L.L. Frankfurt, M. Strikman, J. Ryckebusch, W. Cosyn, M. Sargsyan, and C. Ciofi degli Atti. The analysis presented here was carried out as part of the Jefferson Lab Hall B Data-Mining project supported by the U.S. Department of Energy (DOE). The research was supported also by the National Science Foundation, the Pazy Foundation, the Israel Science Foundation, the Chilean Comisin Nacional de Investigacin Cientfica y Tecnolgica, the French Centre National de la Recherche Scientifique and Commissariat a l'Energie Atomique the French-American Cultural Exchange, the Italian Istituto Nazionale di Fisica Nucleare, the National Research Foundation of Korea, and the UK's Science and Technology Facilities Council. Jefferson Science Associates operates the Thomas Jefferson National Accelerator Facility for the DOE, Office of Science, Office of Nuclear Physics under contract DE-AC05-06OR23177. The raw data from this experiment are archived in Jefferson Lab's mass storage silo.

* Contact Author hen@mit.edu
† On sabbatical leave from Nuclear Research Centre Negev, Beer-Sheva, Israel
‡ Current address: Idaho State University, Pocatello, Idaho 83209
§ Current address: Thomas Jefferson National Accelerator Facility, Newport News, Virginia 23606

[1] O. Hen, G. A. Miller, E. Piasetzky, and L. B. Weinstein, Rev. Mod. Phys. **89**, 045002 (2017).
[2] C. Ciofi degli Atti, Phys. Rept. **590**, 1 (2015).
[3] O. Hen et al. (CLAS Collaboration), Science **346**, 614 (2014).
[4] M. M. Sargsian, Phys. Rev. **C89**, 034305 (2014).
[5] J. Ryckebusch, M. Vanhalst, and W. Cosyn, J. Phys. G **42**, 055104 (2015).
[6] M. Duer et al. (CLAS Collaboration), Nature **560**, 617

(2018).
[7] J. Ryckebusch, W. Cosyn, S. Stevens, C. Casert, and J. Nys (2018), 1808.09859.
[8] L. Frankfurt, M. Sargsian, and M. Strikman, Int. J. Mod. Phys. A **23**, 2991 (2008).
[9] O. Hen, B.-A. Li, W.-J. Guo, L. B. Weinstein, and E. Piasetzky, Phys. Rev. C **91**, 025803 (2015).
[10] B.-A. Li, B.-J. Cai, L.-W. Chen, and J. Xu, Prog. Part. Nucl. Phys. **99**, 29 (2018), 1801.01213.
[11] L. B. Weinstein, E. Piasetzky, D. W. Higinbotham, J. Gomez, O. Hen, and R. Shneor, Phys. Rev. Lett. **106**, 052301 (2011).
[12] O. Hen, A. Accardi, W. Melnitchouk, and E. Piasetzky, Phys. Rev. D **84**, 117501 (2011).
[13] O. Hen, E. Piasetzky, and L. B. Weinstein, Phys. Rev. C **85**, 047301 (2012).
[14] O. Hen, D. W. Higinbotham, G. A. Miller, E. Piasetzky, and L. B. Weinstein, Int. J. Mod. Phys. **E22**, 1330017 (2013).
[15] J.-W. Chen, W. Detmold, J. E. Lynn, and A. Schwenk, Phys. Rev. Lett. **119**, 262502 (2017).
[16] C. Ciofi degli Atti, L.L. Frankfurt, L.P. Kaptari and M.I. Strikman, Phys. Rev. C **76**, 055206 (2007).
[17] B. Schmookler et al. (CLAS Collaboration), Nature **566**, 354 (2019).
[18] A. Tang et al., Phys. Rev. Lett. **90**, 042301 (2003).
[19] E. Piasetzky, M. Sargsian, L. Frankfurt, M. Strikman, and J. W. Watson, Phys. Rev. Lett. **97**, 162504 (2006).
[20] R. Subedi et al., Science **320**, 1476 (2008).
[21] I. Korover, N. Muangma, O. Hen, et al., Phys. Rev. Lett. **113**, 022501 (2014).
[22] R. Schiavilla, R. B. Wiringa, S. C. Pieper, and J. Carlson, Phys. Rev. Lett. **98**, 132501 (2007).
[23] M. M. Sargsian, T. V. Abrahamyan, M. I. Strikman, and L. L. Frankfurt, Phys. Rev. C **71**, 044615 (2005).
[24] M. Alvioli, C. Ciofi degli Atti, and H. Morita, Phys. Rev. Lett. **100**, 162503 (2008).
[25] T. Neff, H. Feldmeier, and W. Horiuchi, Phys. Rev. C **92**, 024003 (2015).
[26] R. Weiss, B. Bazak, and N. Barnea, Phys. Rev. **C92**, 054311 (2015), 1503.07047.
[27] R. Weiss, R. Cruz-Torres, N. Barnea, E. Piasetzky, and O. Hen, Phys. Lett. B **780**, 211 (2018).
[28] R. Weiss, I. Korover, E. Piasetzky, O. Hen, and N. Barnea, Physics Letters B **791**, 242 (2019).
[29] L. L. Frankfurt, M. M. Sargsian, and M. I. Strikman, Phys. Rev. **C56**, 1124 (1997).
[30] C. Colle et al., Phys. Rev. C **92**, 024604 (2015).
[31] C. Colle, W. Cosyn, and J. Ryckebusch, Phys. Rev. **C93**, 034608 (2016).
[32] W. U. Boeglin, L. Coman, P. Ambrozewicz, K. Aniol, J. Arrington, G. Batigne, P. Bosted, A. Camsonne, G. Chang, J. P. Chen, et al. (For the Hall A Collaboration), Phys. Rev. Lett. **107**, 262501 (2011).
[33] M. Duer, O. Hen, E. Piasetzky, L. B. Weinstein, A. Schmidt, I. Korover, E. O. Cohen, and H. Hakobyan (CLAS Collaboration) (2018), 1811.01823.
[34] O. Hen et al. (CLAS Collaboration), Phys. Lett. **B722**, 63 (2013).
[35] J. Ryckebusch, D. Debruyne, P. Lava, S. Janssen, B. Van Overmeire, and T. Van Cauteren, Nucl. Phys. **A728**, 226 (2003).
[36] C. Colle, W. Cosyn, J. Ryckebusch, and M. Vanhalst, Phys. Rev. **C89**, 024603 (2014).
[37] D. Dutta, K. Hafidi, and M. Strikman, Prog. Part. Nucl. Phys. **69**, 1 (2013).
[38] L. Frankfurt, M. Strikman, and M. Zhalov, Phys. Lett. **B503**, 73 (2001).
[39] V. R. Pandharipande and S. C. Pieper, Phys. Rev. **C45**, 791 (1992).
[40] M. M. Sargsian, Int. J. Mod. Phys. **E10**, 405 (2001).
[41] J. Carlson, S. Gandolfi, F. Pederiva, S. C. Pieper, R. Schiavilla, K. E. Schmidt, and R. B. Wiringa, Rev. Mod. Phys. **87**, 1067 (2015).
[42] S. N. More, S. K. Bogner, and R. J. Furnstahl, Phys. Rev. C **96**, 054004 (2017).
[43] L.B. Weinstein, S.E. Kuhn and M. Strikman, Short distance structure of nuclei: Mining the wealth of existing jefferson lab data, DOE Grant DE-SC0006801 (2016).
[44] H. Hakobyan et al., Nucl. Instrum. Meth. **A592**, 218 (2008).
[45] B. A. Mecking et al., Nucl. Instrum. Meth. **A503**, 513 (2003).
[46] W. P. Ford, S. Jeschonnek, and J. W. Van Orden, Phys. Rev. **C90**, 064006 (2014).
[47] W. Cosyn, Private Communications (2018).
[48] E. O. Cohen et al. (CLAS Collaboration), Phys. Rev. Lett. **121**, 092501 (2018), 1805.01981.
[49] C. Ciofi degli Atti and S. Simula, Phys. Rev. C **53**, 1689 (1996).
[50] R. B. Wiringa, V. G. J. Stoks, and R. Schiavilla, Phys. Rev. C **51**, 38 (1995).
[51] A. Gezerlis, I. Tews, E. Epelbaum, S. Gandolfi, K. Hebeler, A. Nogga, and A. Schwenk, Phys. Rev. Lett. **111**, 032501 (2013), 1303.6243.
[52] A. Gezerlis, I. Tews, E. Epelbaum, M. Freunek, S. Gandolfi, K. Hebeler, A. Nogga, and A. Schwenk, Phys. Rev. **C90**, 054323 (2014), 1406.0454.
[53] E. Epelbaum, H.-W. Hammer, and U.-G. Meissner, Rev. Mod. Phys. **81**, 1773 (2009), 0811.1338.
[54] T. De Forest, Nucl. Phys. **A392**, 232 (1983).
[55] J. J. Kelly, Phys. Rev. **C70**, 068202 (2004).
[56] J. L. Friedes, H. Palevsky, R. L. Stearns, and R. J. Sutter, Phys. Rev. Lett. **15**, 38 (1965).

Supplementary Materials

Formalism

In the absence of FSI, assuming scattering from an SRC pair, the $A(e,e'np)$ and $A(e,e'pp)$ measured cross-sections can be written as:

$$\begin{aligned} A(e,e'pp) &\propto \#pp_A \cdot 2 \cdot \sigma_{ep}, \\ A(e,e'np) &\propto \#np_A \cdot \sigma_{en}, \end{aligned} \tag{3}$$

where $\#pp_A$ ($\#np_A$) is the number of proton-proton (neutron-proton) pairs in nucleus A and σ_{ep} (σ_{en}) is the electron-proton (electron-neutron) cross-section.

With FSI, one should take into account contributions from all NN-SRC pairs that can lead to the same measured final state, the effects of nuclear transparency and SCX.

Using the notation defined in the main text for the SCX probabilities, Eq. 3 can be extended as:

$$\begin{aligned} A(e,e'pp) \propto & \#pp_A \cdot 2\sigma_{ep} \cdot P_A^{pp} \cdot T_{A,pp} + \\ & \#np_A \cdot \sigma_{en} \cdot p_A^{[n]p} \cdot T_A^* + \\ & \#pn_A \cdot \sigma_{ep} \cdot P_A^{p[n]} \cdot T_A^*, \\ A(e,e'np) \propto & \#np_A \cdot \sigma_{en} \cdot P_A^{np} \cdot T_{A,np} + \\ & \#pp_A \cdot 2\sigma_{ep} \cdot P_A^{[p]p} \cdot T_A^* + \\ & \#nn_A \cdot 2\sigma_{en} \cdot P_A^{n[n]} \cdot T_A^*, \end{aligned} \tag{4}$$

where T_{pp} (T_{np}) is the nuclear transparency for two protons (neutron-proton) and T^* is the transparency associated with a SCX process.

Eq. 2 in the main text can be obtained from Eq. 4 above by forming the $A(e,e'pp)$ / $A(e,e'pn)$ ratio and assuming that $T^* = \frac{1}{2}(T_{pp}+T_{np}) = T_{pp} = T_{np}$. The latter approximation is valid when considering high-Q^2 reactions with a high energy leading proton/neutron that has the same nuclear transparency for pp and np pairs [31, 35].

Following Ref. [28], and adopting the kinematical notations of Fig. 1 of the main text, the GCF calculated cross-section for the $A(e,e'NN)$ process without FSI can be expressed as:

$$\begin{aligned} &\frac{d^8\sigma}{dQ^2 dx_B d\phi_e d^3\vec{p}_{CM} d\Omega_{rec}} = \\ &\frac{\sigma_{eN}}{32\pi^4} \times n(\vec{p}_{CM}) \times \sum_\alpha C_\alpha |\tilde{\varphi}^\alpha(|\vec{p}_{CM} - 2\vec{p}_{rec}|)|^2 \times \\ &\frac{E_N E_{rec} p_{rec}^2}{|E_{rec}(p_{rec} - Z\cos\theta_{Z,rec}) + E_N p_{rec}|} \times \frac{\omega}{2E_{beam}E_e x_B}, \end{aligned} \tag{5}$$

where the subscript 'N' ('rec') stands for the leading (recoil) nucleon, 'e' stands for the scattered electron, $\vec{Z} = \vec{q} + \vec{p}_{CM}$ and $\theta_{Z,rec}$ is the angle between $\vec{Z}$ and $\vec{p}_{rec}$.

The second line shows the GCF factorization to an off-shell electron-nucleon cross section σ_{eN} (taken from Ref. [54], using the form factor parameterization of Ref. [55]), times an SRC pair center-of-mass momentum distribution $n(\vec{p}_{CM})$ (given by a three-dimensional Gaussian with width of 150 ± 20 MeV/c [36, 48, 49]), times a summation over all SRC pairs that can contribute to a given NN final state (without SCX). The index α represents the quantum numbers of an SRC pair such that for $(e,e'pp)$ α stands for spin-0 pp pairs while for $(e,e'pn)$ it is summed over both spin-0 and spin-1 pn pairs. The functions $\tilde{\varphi}^\alpha$ are the universal SRC pairs relative momentum distributions obtained by solving the zero-energy two-body Schrodinger equation of a NN pair in quantum state α using a given NN potential model. C_α are nuclear contact terms that determine the relative abundance of SRC pairs with a given quantum state. For pp (nn) pairs C_α is equal to twice the nuclear contact for pp-SRC (nn-SRC) pairs. The third line is simply a Jacobian term.

The total measured two-nucleon knockout cross-section, $\sigma^{GCF}_{A(e,e'NN)}$, is obtained by integrating Eq. 5 over the experimental acceptance as detailed below.

FSI can be introduced to the GCF calculation in a similar manner as in Eq. 4 using:

$$\begin{aligned} \sigma^{Exp}_{A(e,e'pp)} = & \sigma^{GCF}_{A(e,e'pp)} \cdot P_A^{pp} \cdot T_{A,pp} + \\ & \sigma^{GCF}_{A(e,e'np)} \cdot p_A^{[n]p} \cdot T_A^* + \\ & \sigma^{GCF}_{A(e,e'pn)} \cdot P_A^{p[n]} \cdot T_A^*, \\ \sigma^{Exp}_{A(e,e'np)} = & \sigma^{GCF}_{A(e,e'np)} \cdot P_A^{np} \cdot T_{A,np} + \\ & \sigma^{GCF}_{A(e,e'pp)} \cdot P_A^{[p]p} \cdot T_A^* + \\ & \sigma^{GCF}_{A(e,e'nn)} \cdot P_A^{n[n]} \cdot T_A^*. \end{aligned} \tag{6}$$

Calculation details

The evaluation of Eq. 2 in the main text, and the estimation of its uncertainties, was done following [3], using a Monte-Carlo technique where its PDF was extracted from repeated calculations using different input values. In each calculation the values of the different parameters (experimental cross-section, SCX probabilities etc.) were randomly chosen from a Gaussian distribution centered at the measured or calculated value with width (1σ) that equaled their associated uncertainties. The cross-section ratios, R, are listed in Table II of the main text, the SCX probabilities are listed in Table III below (based on the calculations of Ref. [31]). Notice that all probabilities (for protons, neutrons, leading, and recoil) increase with A. The probabilities for the lower-momentum re-

coil nucleons are larger than those for the leading nucleons. The SCX probabilities for protons are larger than for neutrons. For the kinematics of the current measurement $\sigma_{p/n} = \frac{\sigma_{ep}}{\sigma_{en}} = 2.30 \pm 0.15$. For asymmetric nuclei $\eta_A = \frac{\#nn_A}{\#pp_A}$ was drawn from a uniform distribution between unity and the combinatorial ratio of possible nn and pp pairs in a given asymmetric nucleus. The resulting FSI-corrected pp/np SRC pairs ratio, presented in Fig. 3 of the main text, show the most-probable value, with confidence bands enclosing 68% of the PDF.

The GCF results shown in Fig. 2 of the main text were obtained by using a Monte-Carlo event generator to integrate Eq. 5 over the experimental acceptance by considering only kinematics where the scattered electron, knockout nucleon and recoil proton would all have been detected in CLAS (i.e., the momentum vectors all point to active regions in CLAS), and furthermore pass the event selections cuts listed in Table I of the main text. Transparency and SCX effects were introduced to the integrated cross-section using Eq. 6. The uncertainty on the calculation was estimated by repeating the calculation many times while varying the input parameters to Eq. 6 and 5 by their uncertainties detailed in the text, and extracting the 68% and 95% confidence intervals of the calculation due to these variations, similar to the procedure described above for Eq. 2 of the main text.

TABLE III: The SCX probabilities for different NN pairs and nuclei. The nucleons in brackets underwent a SCX interaction, the ones not in brackets did not. Thus, $P^{[p]n}$ indicates the probability that the proton in a knocked-out pn pair undergoes a SCX reaction and the neutron does not.

	C	Al	Fe	Pb
P^{pp}	0.908 ± 0.006	0.897 ± 0.009	0.891 ± 0.010	0.860 ± 0.013
$P^{[p]p}$	0.041 ± 0.003	0.046 ± 0.004	0.048 ± 0.005	0.059 ± 0.006
$P^{p[p]}$	0.048 ± 0.003	0.054 ± 0.005	0.057 ± 0.006	0.074 ± 0.007
$P^{[pp]}$	0.003 ± 0.0002	0.004 ± 0.0003	0.004 ± 0.0003	0.007 ± 0.0006
$P^{p[n]}$	0.041 ± 0.003	0.047 ± 0.005	0.047 ± 0.005	0.047 ± 0.005
$P^{[p]n}$	0.035 ± 0.002	0.043 ± 0.004	0.046 ± 0.005	0.061 ± 0.006
P^{np}	0.922 ± 0.005	0.907 ± 0.008	0.903 ± 0.009	0.887 ± 0.010
$P^{[n]p}$	0.035 ± 0.002	0.040 ± 0.004	0.040 ± 0.004	0.040 ± 0.004
$P^{n[p]}$	0.041 ± 0.003	0.051 ± 0.005	0.054 ± 0.006	0.072 ± 0.008
$P^{[np]}$	0.002 ± 0.0001	0.003 ± 0.0002	0.004 ± 0.0003	0.005 ± 0.0004
$P^{n[n]}$	0.048 ± 0.003	0.050 ± 0.005	0.049 ± 0.005	0.048 ± 0.005